Int J Adv Manuf Technol (2017) 88:2201–2210
DOI 10.1007/s00170-016-8922-8

ORIGINAL ARTICLE

The seam position detection and tracking for the mobile welding robot

Xueqin Lü[1] · **Ke Zhang**[2] · **Yixiong Wu**[2]

Received: 27 January 2016 / Accepted: 12 May 2016 / Published online: 28 May 2016

Abstract To solve the problems that the current seam tracking process cannot find the weld line and the control method based on the kinematic model of welding mobile robot leads to low accuracy, a method for searching the welding seam is designed firstly. By this method, the initiation point of the weld line can be found and the attitude of the robot parallel to the weld line can be adjusted automatically. Secondly, for improving the tracking precision and anti-interference performance, a new controller based on the kinematic and dynamic model of the mobile welding robot is designed. To deal with the partial uncertainty and the disturbances of welding process, this controller combines the sliding mode variable structure control and low-pass filter, so that it is able to complete the controlling of cross-slider and wheels coordinately. The stability and convergence of the designed controller are proved through the use of Lyapunov theory. The effectiveness of the proposed method is verified by simulation and experiments. In the seam tracking process, the welding torch is able to track the welding seam well and the robot moves steadily without any obvious chattering.

Keywords Mobile welding robot · Weld line position detection · Automatic detection system · LPF

✉ Xueqin Lü
lvxueqin@shiep.edu.cn

[1] School of Automation Engineering, Shanghai University of Electric Power, Shanghai, China

[2] School of Materials Science and Engineering, Shanghai Jiao Tong University, Shanghai, China

1 Introduction

In welding process, there are many limitations for acquiring continuous, stable quality and increasing productivity because the welding quality depends on worker's skillfulness and other factories, which not only included the thickness of the materials to be welded, the chemical element composition of the welded material, and the surface treatment of the workpiece but also included welding method, welding speed, and welding path, especially automatic finding of the initial welding location and seam tracking of the welding seam in real time [1–4]. A rapid development in computer technology and robot technology has led to great improvement in the automated welding process [5–7].

To realize an automatic welding process, nowadays, a mobile type of welding robot is used for welding line. But, it cannot find the position of the weld line automatically. The first major issue in welding robotics is to find the position of the weld line [8–12]. In most practical applications, such as mobile welding robot, the robot task is to track a given path with constant line speed and the smallest possible error [13–16].

After finding the weld line, the robot starts the weld seam tracking process. Accurate path tracking has received considerable attention in recent years. It is a task that is difficult to achieve for industrial robots. An application where this plays an important role is seam tracking in robot welding field. So many scholars have carried out research on the seam tracking and have achieved a lot of fruitful research results [17, 18]. Although significant achievements have been made in the area of seam tracking, reliable application techniques for robots are still needed. The majority of the existing methods only consider the kinematic models and less consider the dynamic models.

In this paper, to realize an automatic welding process, a mobile type of welding robot is used. At the same time, we simply introduce an algorithm for finding the position of the weld line

automatically using the laser sensor, and an improved sliding mode control (SMC) seam tracking method with a low-pass filter for mobile welding robot is also elaborated.

2 The configuration and detection principle of a laser displacement sensor

A seam tracking sensor in an automation welding system is necessary [19–21]. Although a vision sensor was the most outstanding technique with non-contact, quick processing, and anti-interference characteristic, the image processing is very complex. This process reduces real-time processing, thus affecting the accuracy of seam tracking [22]. A laser displacement sensor has become an indispensable tool in the robotics community. A less common but growing application field for laser range finders is a seam tracking system. The laser displacement sensor offers many advantages over other types of sensors. Their advantages include high measurement accuracy and simplicity of data processing when compared with visual tracking.

Figure 1 shows the laser displacement sensor (LDS). The sensor is comprised of a light-emitting element, a main processing circuit, and a position sensitive detector (PSD), which detects targets using triangulation (shown in Fig. 1b). A LED is used as the light-emitting element. As shown in Fig. 2, one-dimensional PSD signal detection and processing circuit consists of the preamplifier, the adder, the subtractor, and the divider. IC_1, IC_2, IC_3, and IC_4 are the high-precision operational amplifier, and AD538 is the analog divider [23].

The surface condition of the target can affect the distribution of light quantity, which causes slight variations in measured values. Therefore, the linear characteristics are a plot of the error in the analog output in the measurement range. The error of the LED displacement sensor increases when the surface of the measured object has a low reflectance (black) or is glossy. But in this paper, the welding surface is smooth plane; the LED sensor enables stable highly accurate displacement measurement, neglecting the light quantity distribution of the beam spot. The scanning principle of the groove detection was listed in the literature [24].

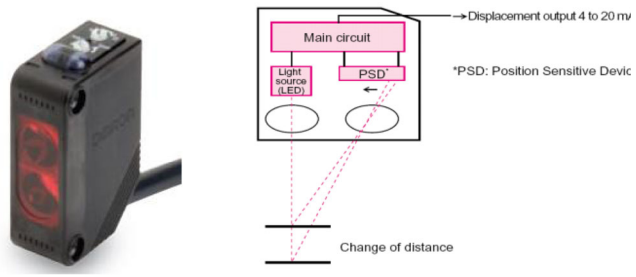

(a) (b)

Fig. 1 Laser displacement sensor. **a** LDS configuration. **b** Principle of detection

3 The mobile welding robot and detection principle

The general structure of the robot is shown in Fig. 3 [25]. This robot consists of a sensor system, a PC processor, a controller, welding equipment, two driving wheels, two passive auxiliary wheels, etc. Meanwhile, all essential control and electrical components are implemented on the internal drive unit. The main difference and performance of this robot with respect to similar ones is its mechanical structure and driving mechanism. The robot consists of two DC servo motors that actuated the main driving wheels parallel to each other and the other two stepper motors that actuated the driving cross-sliders as a fine-tuning mechanism. The torch in front of the laser sensor is driven by a rotary motor to perform weld groove scanning. The geometric center C of the body is the center of mass. The passive wheels prevent the robot from tipping over as it moves on a plane. In this paper, we neglect the effect of auxiliary wheel motion to the whole system.

4 Modeling analysis

4.1 The kinematic analysis

The kinematic scheme of a mobile welding robot depicted in Fig. 4 is a typical example of non-holonomic mechanical systems. To describe the robot motion, several reference coordinate systems are depicted. AXY is the reference coordinate system; $BX1Y1$ is the coordinate system fixed to the mobile robot; B, the middle between the right and left driving wheels, is the origin of the mobile robot; W is the welding torch, and C is the centroid of the robot body. a is the distance from B to S; b is the distance from S to W (original position); $2l$ is the distance between the two driving wheels, and r is the radius of the wheel. In the two-dimensional Cartesian space, the pose of the robot is represented by the vector $P=[xy\theta]^T$, where $(x, y)^T$ is the coordinate of $BX1$ in the reference coordinate system, and the heading direction θ is taken counterclockwise from the AX-axis. The currently linear velocity and angular velocity of the robot are respectively denoted by v and ω. Suppose the welding torch is required to track a reference trajectory, we have to coordinate control cross-sliders and two driving wheels to make the welding torch track the weld seam with a reference velocity.

As the longitudinal and lateral motions are not coupled, independent of each other, so the control algorithms can be designed vertically and horizontally,

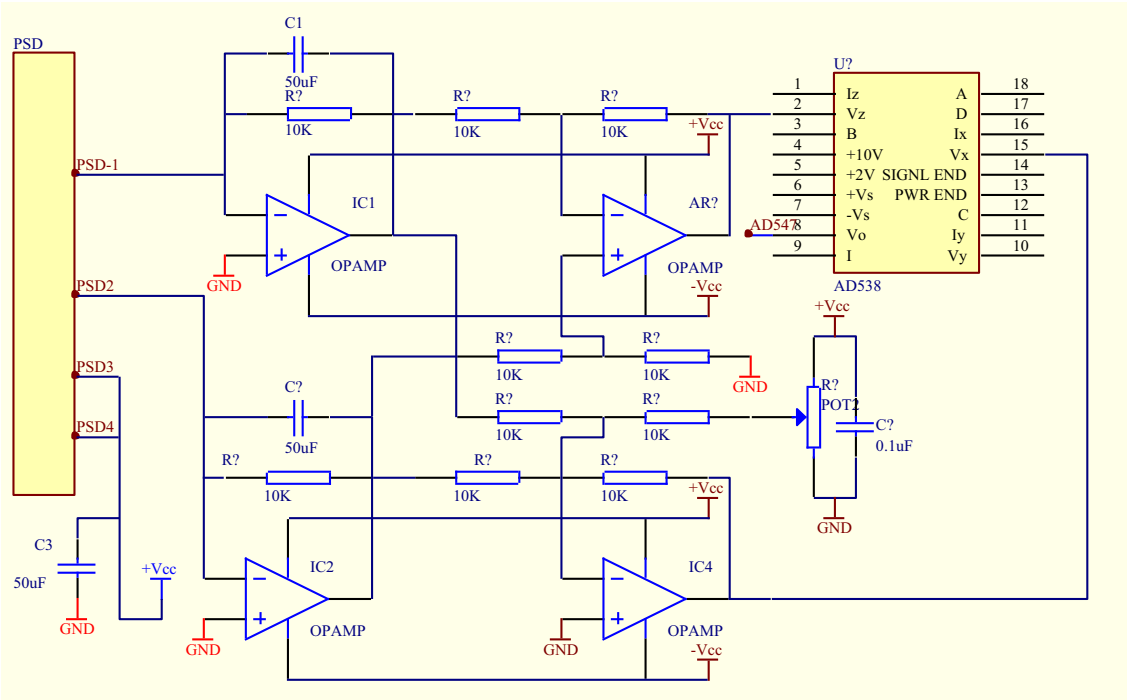

Fig. 2 Main circuit of one-dimensional PSD

respectively. This paper only studies the control of the lateral cross-slider.

It is assumed that the wheels of the robot do not slide; that is, the mobile robot can only move in the direction normal to the axis of the driving wheels, so we can obtain the following non-holonomic constrains equation

$$\dot{x}\sin\theta - \dot{y}\cos\theta = 0 \tag{1}$$

Fig. 3 Architecture diagram of the robot system

Take point B as the reference point to establish the kinematic model of the welding mobile robot, and the position of the kinematic mode of the mobile welding robot is follows:

$$\begin{bmatrix} \dot{x} \\ \dot{y} \\ \dot{\theta} \end{bmatrix} = \begin{bmatrix} \cos\theta & 0 \\ \sin\theta & 0 \\ 0 & 1 \end{bmatrix} \begin{bmatrix} v \\ \omega \end{bmatrix} \tag{2}$$

The velocity of the welding torch (point W) would be impact not only by the velocities of the two driving wheels but also by the velocity of the horizontal cross-slider. Therefore, in this paper, we also take into account the velocity of the horizontal cross-slider, which will improve the precision of seam tracking. Suppose $S_b(t)$ is the distance between S and W, then the linear velocity of the horizontal cross-slider is $S_b(t)$. From Fig. 4, the posture of the welding torch at point W can be described as follows:

$$\begin{bmatrix} x_W \\ y_W \\ \theta_W \end{bmatrix} = \begin{bmatrix} x \\ y \\ \theta \end{bmatrix} + \begin{bmatrix} -L\cos\alpha & -\left[L\sin\alpha + S_{sp}(t)\right] & 0 \\ -\left[L\sin\alpha + S_{sp}(t)\right] & L\cos\alpha & 0 \\ 0 & 0 & 1 \end{bmatrix} \begin{bmatrix} \cos\theta \\ \sin\theta \\ \alpha \end{bmatrix} \tag{3}$$

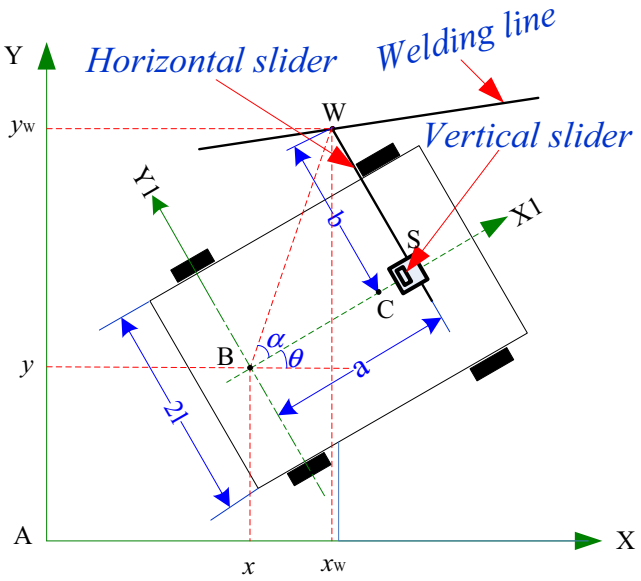

Fig. 4 Kinematical scheme of the mobile welding robot

where L is the distance from B to W and α is $\angle CBW$.

4.2 Dynamics of mobile welding robot

Suppose moving on a horizontal plane; the welding mobile robot system with a non-holonomic constraint can be described by the following dynamic equations:

$$M(q)\ddot{q} + V_m\left(q,\dot{q}\right)\dot{q} + F\left(\dot{q}\right) + G(q) + \tau_d = B(q)T - A^T(q)\lambda \quad (4)$$

where q, $\dot{q}$, and $\ddot{q}$ are the vectors of robot body positions, velocities, and accelerations, respectively; $M(q)$ is the system inertia matrix; $V(q,\dot{q})$ is the centripetal force matrix which refers to the position and the speed; $F(\dot{q})$ is the surface friction; $G(q)$ is the gravitational force; τ_d is the uncertain modeling matrix and unknown disturbance; $B(q)$ is the input transformation matrix; T is the input moment vector; $A(q)$ is the constraint matrix; and λ is the binding force vector.

Ignore the friction of the surface friction and the binding force vector and treat them as an uncertain modeling matrix. Then, the dynamic model of the welding mobile robot is change into the following:

$$M(q)\ddot{q} + V_m\left(q,\dot{q}\right)\dot{q} + \Delta\left(q,\dot{q}\right) + \tau_d = B(q)T \quad (5)$$

where

$$M(q) = \begin{bmatrix} m + \frac{2I_d}{r} & 0 & 0 \\ 0 & m + \frac{2I_d}{r} & 0 \\ 0 & 0 & I + \frac{2I_d l}{r^2} \end{bmatrix};\quad B(q) = \frac{1}{r}\begin{bmatrix} \cos\theta & \cos\theta \\ \sin\theta & \sin\theta \\ l & -l \end{bmatrix};$$

$$V_m\left(q,\dot{q}\right) = \begin{bmatrix} \frac{2I_d}{r^2}\tan\theta\cdot\dot{\theta} + \frac{2c_m}{r^2} & 0 & 0 \\ 0 & -\frac{2I_d}{r^2}c\tan\theta\cdot\dot{\theta} + \frac{2c_m}{r^2} & 0 \\ 0 & 0 & \frac{2c_m l^2}{r^2} \end{bmatrix}$$

$\Delta(q,\dot{q})$ is the uncertain modeling matrix.

5 The strategy of finding the seam position automatically

The robot is put on one side of the welding line. Figure 5a, b serves to obtain the entrance angle (γ) between the moving direction and the welding line. When the sensor detects the groove, the control part begins to calculate the entrance angle according to the position information from the sensor. At the same time, γ is fed back to the driving wheels. Then, the angle value is regarded as the initial condition for finding the position of the weld line. The robot moves back in a straight line for a distance S. In Fig. 5c, d, the robot begins to turn. Φ is regarded as the turning angle of the steering wheels. During this period, the angle changes from 0 to φ_0 gradually. In Fig. 5e, the robot moves along a circular path. In Fig. 5f, the turning angle changes from φ_0 to 0. At the

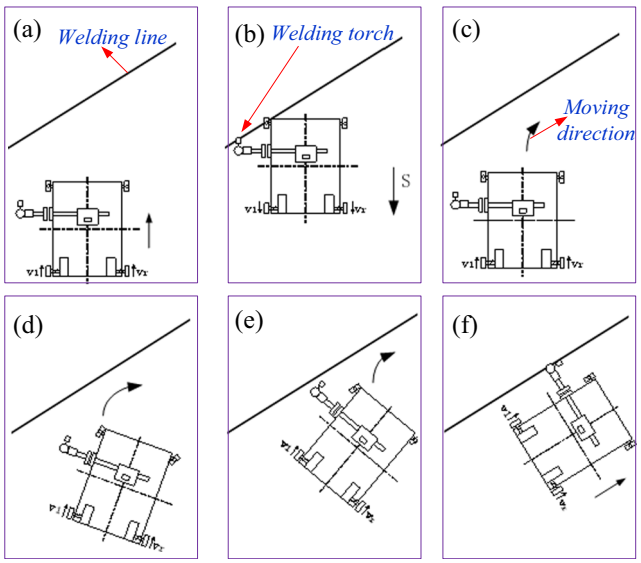

Fig. 5 **a**–**f** Diagram of the operating schedule for a tracing process

end of this stage, the robot runs parallel to the weld center line in an appropriate way and the welding torch coincides with the welding line.

Figure 6 shows the diagram of the automatic mobile welding robot finding the seam line. The whole turning process is separated into three stages. Those correspond to the process in Fig. 5c–f. The speed rate (v) of the robot and the mean angular velocity of the driving wheels (ω) are always constant. When the turning time is determined, the steering angle is also determined. The initial moving direction of the robot acts as the positive direction axis. The central point of the rear axis acts as the origin of the coordinates.

At the first turning stage, the robot starts to move from the start point O to O_1. In this process, the mean turning angle changes from 0 to ϕ. The turning radius (R) changes from $+\infty$ to 0 correspondingly. The turning angle is $\phi=(\phi_1+\phi_2)/2=\omega_1 t$ (rad) and the turning radius at time t is $R=l/\phi=l/\omega_1 t$, where ω_1 is the angular velocity of the driving wheels from O to O_1 (rad/s) and l is the distance between the axes of the turning wheels and the driving wheels (mm). At the first moment, the initial values are all equal to zero and then the trajectory locomotion on O–O_1 can be calculated as follows [24]:

$$\begin{cases} x_{O\text{–}O_1} = \int_0^t v\sin\left[\frac{v\omega_1}{2l}\tau^2\right]d\tau = \sqrt{\frac{\pi v l}{\omega_1}}\text{Fresnel } S\left[\sqrt{\frac{v\omega_1}{l\pi}}t\right] \\ y_{O\text{–}O_1} = \int_0^t v\cos\left[\frac{v\omega_1}{2l}\tau^2\right]d\tau = \sqrt{\frac{\pi v l}{\omega_1}}\text{Fresnel } C\left[\sqrt{l\frac{v\omega_1}{L\pi}}t\right] \end{cases} \quad (6)$$

When the robot arrives at O_1, it starts to move along the circular path with constant radius $R_0=l/\phi_0$. As can be seen in Fig. 7, the coordinate of point M, which is an arbitrary point at the stage of O_1–O_2 can be calculated as

$$\begin{cases} x_{O_1\text{–}O_2} = x_1 + 2R_0\sin(\beta/2)\sin(\alpha_1+\beta/2) \\ y_{O_1\text{–}O_2} = y_1 + 2R_0\sin(\beta/2)\cos(\alpha_1+\beta/2) \end{cases} \quad (7)$$

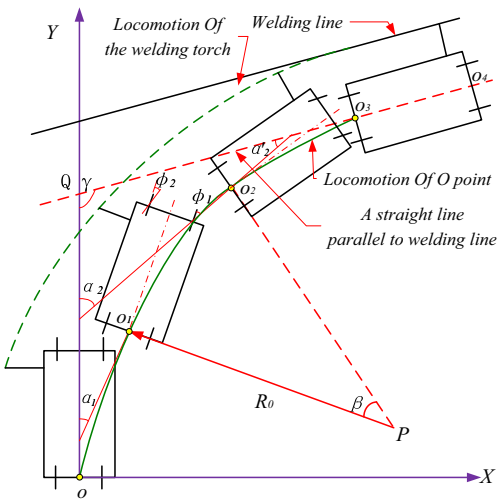

Fig. 6 Diagrammatic sketch of the tracing welding line

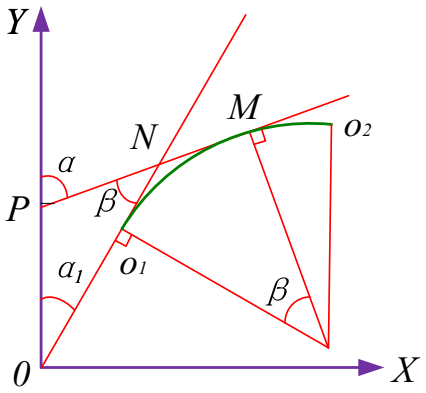

Fig. 7 Geometry relationship at O_1–O_2

where α_1 is the angle between y-axis and O_1 point tangent line on O–O_1.

Using the same calculation principle, we can get the locomotion equation from O_2 to O_3 as follows:

$$\begin{cases} x_{O_2\text{–}O_3} = x_2 - \sqrt{\frac{l\pi v}{\omega_1}}\left(\cos\left[\frac{v{\phi_0}^2+2l\gamma\omega_1}{2l\omega_1}\right]\text{Fresnel } S\left[\sqrt{\frac{v\omega_1}{l\pi}}t'\right]\right. \\ \qquad \left. -\text{Fresnel } C\left[\sqrt{\frac{v\omega_1}{l\pi}}t'\right]\sin\left[\frac{v{\phi_0}^2+2l\gamma\omega_1}{2l\omega_1}\right]\right) \\ y_{O_2\text{–}O_3} = y_2 - \sqrt{\frac{l\pi v}{\omega_1}}\left(\cos\left[\frac{v{\phi_0}^2+2l\gamma\omega_1}{2l\omega_1}\right]\text{Fresnel } C\left[\sqrt{\frac{v\omega_1}{l\pi}}t'\right]\right. \\ \qquad \left. +\text{Fresnel } S\left[\sqrt{\frac{v\omega_1}{l\pi}}t'\right]\sin\left[\frac{v{\phi_0}^2+2l\gamma\omega_1}{2l\omega_1}\right]\right) \end{cases} \quad (8)$$

where t' is the time parameter when the steering angle is changing; (x_1,y_1) and (x_2,y_2) are the coordinates O_1 and O_2, respectively, which can be expressed as

$$\begin{cases} x_1 = \sqrt{\frac{\pi v l}{\omega_1}}Fresnel\ S\left[\sqrt{\frac{v}{l\pi\omega_1}}\phi_0\right] \\ y_1 = \sqrt{\frac{\pi v l}{\omega_1}}Fresnel\ C\left[\sqrt{\frac{v}{l\pi\omega_1}}\phi_0\right] \end{cases} \quad (9)$$

$$\begin{cases} x_2 = x_1 + 2R_0\sin\left[\frac{\pi-\gamma-(v{\phi_0}^2/l\omega_1)}{2}\right]\sin\left(\frac{\pi-\gamma}{2}\right) \\ y_2 = y_1 + 2R_0\sin\left[\frac{\pi-\gamma-(v{\phi_0}^2/l\omega_1)}{2}\right]\cos\left(\frac{\pi-\gamma}{2}\right) \end{cases} \quad (10)$$

6 Welding seam tracking method

From the robotics viewpoint, the mobile welding robot is a multi-input\multi-output (MIMO) non-linear system [26, 27]. SMC, as one of the most robust control approaches, makes the control system insensitive to parametric uncertainties and norm-bounded disturbances [28]. On the other hand, the

control performance is limited either due to its high gain chattering nature or due to the introduction of smoothing technique approach as the trade-off.

In order to overcome chattering of SMC, Zhu et al. [29] developed a sliding mode controller with a low-pass filter for robot manipulators by inserting a low-pass filter (LPF) in front of the plan, the low-pass filter weaken the chattering of the sliding mode controller, and the precise of the trace tracking can be converged to zero exponentially under the existence of parameter uncertainties and disturbances. The author's team previously proposed a sliding mode control scheme with smooth continuous function, which guarantees the smoothness of the control signal and the exponential error convergence for mobile welding robot [30, 31].

A novel control algorithm to achieve seam tracking of a mobile robot with non-holonomic constraints is proposed. This algorithm uses the theories of sliding mode for robust control to compensate for unknown disturbances applied to mobile welding robot and a LPF to eliminate the high-frequency chattering control signal.

In order to further weaken the influence of the chattering and increase the precise of the trace tracking of the mobile welding robot, the traditional switching function is replaced by smooth continuous function. It has the ability to solve the seam tracking problem based on the dynamic modeling of the mobile welding robot. Particularly, the dynamic performance of the cross-slider is also considered.

Adding a low-pass filter at the output of the sliding mode controller, the high-frequency control signal chattering can be filtered out effectively. The control system based on the sliding mode variable structure is shown in Fig. 8.

According to the matrix theory, the dynamic (Eq. (5)) of the robot can be rewritten to the following form:

$$M'(q)\ddot{q} + V'_m\left(q,\dot{q}\right)\dot{q} + \Delta'\left(q,\dot{q}\right) + \tau'_d = T \tag{11}$$

where $M'(q) = \overline{B}(q)M(q)$, $V'_m(q,\dot{q}) = \overline{B}(q)V_m(q,\dot{q})$, and $\overline{B}(q) = \left[B^T(q)B(q)\right]^{-1}B^T(q)$. $\Delta'(q,\dot{q})$ and τ'_d are still treated as the uncertain modeling matrix and unknown disturbance, respectively.

Define a disturbance vector as $d = \Delta'(q,\dot{q}) + \tau'_d$. Then, Eq. (11) is rewritten by another form as follows:

$$M'(q)\ddot{q} + V'_m\left(q,\dot{q}\right)\dot{q} + d(t) = T \tag{12}$$

The matrixes in Eq. (12) satisfy the following properties:

Property 1 $M'(q)$ is the symmetric positive definite matrix;

Property 2 Boundedness: matrix functions $M'(q)$ and $V'(q)$ are uniformly bounded not only to q but also to $\dot{q}$;

Property 3 $(M'(q)–2V'(q))$ is the skew-symmetric matrix, as to an arbitrary vector ξ, $\xi^T\left[M'(q)–2V'(q,\dot{q})\right]\xi = 0$

Property 4 Linear characteristic: if the constant coefficients of matrix functions denoted a vector θ, then we can define a proper matrix $\varphi(q,\dot{q},v,a)$. Equation (12) can be rewritten by another form as follows:

$$M'(q)a + V'_m\left(q,\dot{q}\right)v + d(t) = \varphi(q,\dot{q},v,a)\theta \tag{13}$$

where v is the velocity vectors and a is the acceleration vectors.

Adopt a low-pass filter as follows [29]:

$$Q(s) = \frac{\lambda_i}{s_i + \lambda_i},\ (\lambda_i > 0.) \tag{14}$$

From Fig. 8, there is $\dot{\tau} + \wedge\tau = \wedge u$, where $\wedge = \mathrm{diag}(\lambda_1, \lambda_2,\ldots, \lambda_n)$; $\lambda_i > 0$ $(i = 1, 2,\ldots, n)$, where n is the number of

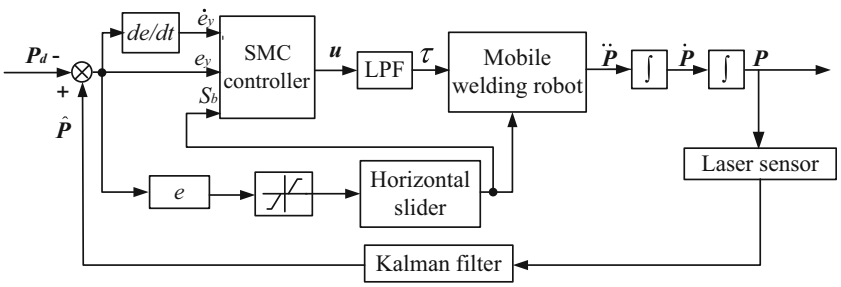

Fig. 8 Sliding mode control with filter

control input signal. Then, Eq. (12) can be rewritten as another form

$$M''\ddot{q} + \dot{M}'\ddot{q} + V'\ddot{q} + V'\dot{q} + \Lambda M''\ddot{q} + \Lambda V'\dot{q} = \Lambda u \tag{15}$$

Define the tracking error as $e(t) = q(t) - q_d(t)$, where $q_d(t)$ is the tracking trajectory.

Define the sliding mode function, which will determine the motion of the system after the system state reached the sliding mode, as follows:

$$s(t) = \ddot{e} + \Lambda_1\dot{e} + \Lambda_2 e \tag{16}$$

where $\Lambda i = \mathrm{diag}(\lambda_{i1}, \lambda_{i2}, \ldots, \lambda_{in})$; $\lambda_{ij} > 0$ $(i = 1, 2; j = 1, 2, \ldots, n)$, where n is the number of control input signal.

Construct the Lyapunov function as $L = \frac{1}{2}s^T M' s$. Because $M'(q)$ is a symmetric positive definite matrix, that is $s^T M' s = \dot{s}^T M' s$, and based on property 3, there is $s^T \left[\dot{M}'(q) - 2V'(q,q)\right] = 0$ and then

$$\begin{aligned} \dot{L} &= \frac{1}{2}\left(s^T M'\dot{s} + s^T \dot{M} s + \dot{s}^T M' s\right) \\ &= s^T M'\dot{s} + \frac{1}{2}s^T \dot{M} s \\ &= s^T\left(M'\dot{s} + V' s\right) \\ &= s^T\left[M'\left(\ddot{q} - \ddot{q}_d + \Lambda_1\ddot{e} + \Lambda_2\dot{e}\right) + V'\left(\dot{e} + \Lambda_1 e + \Lambda_2 e\right)\right] \end{aligned} \tag{17}$$

From Eq. (15), there is

$$\begin{aligned} M'\ddot{q} &= \Lambda u - M'\ddot{q} - V'\ddot{q} - V'q - \Lambda M'\ddot{q} - \Lambda V'\dot{q} \\ &= \Lambda u - \left(\dot{M}' + \Lambda M'\right)\ddot{q} - (V' + \Lambda V')\dot{q} - V'\ddot{q} \end{aligned} \tag{18}$$

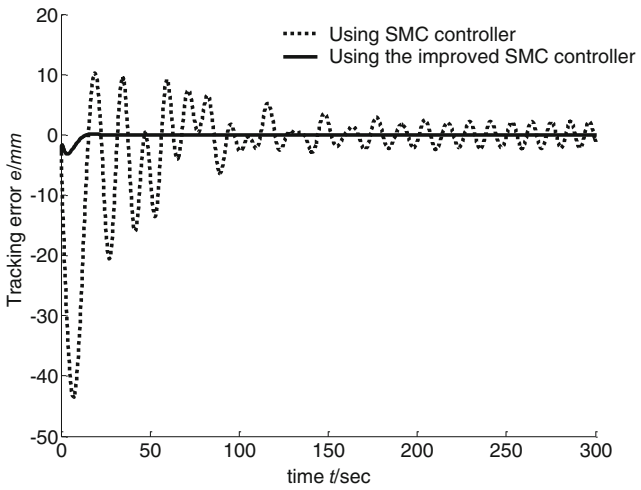

Fig. 9 Seam tracking error

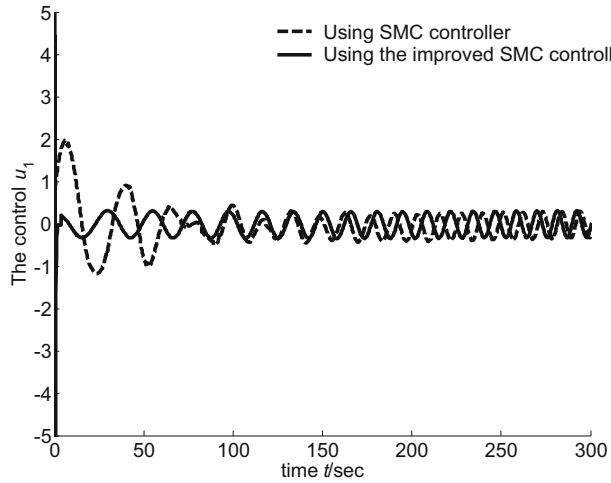

(a) Control output u_1

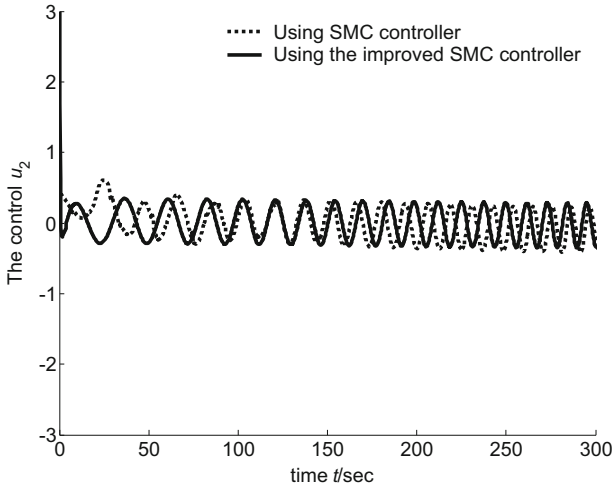

(b) Control output u_2

Fig. 10 Control outputs u_1 (**a**) and u_2 (**b**)

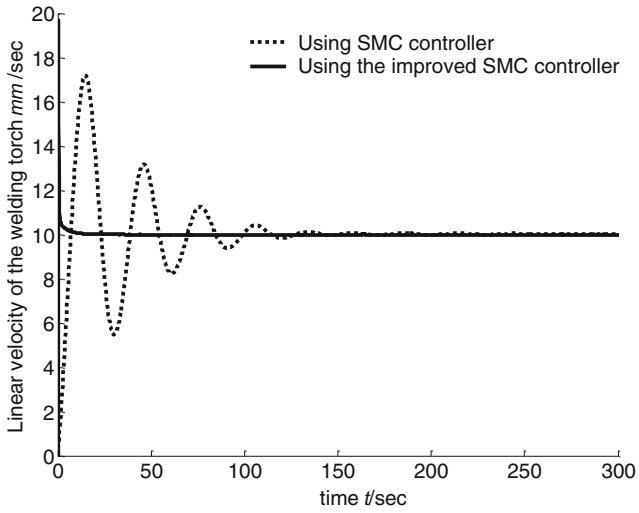

Fig. 11 Linear velocity of the welding torch

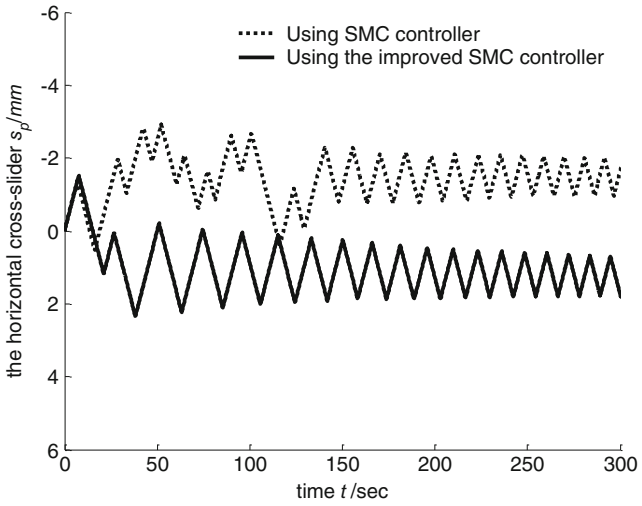

Fig. 12 Horizontal cross-slider (s_p)

Then, Eq. (17) can be written as

$$\begin{aligned}\dot{L} &= s^T\left[\Lambda u-\left(\dot{M}'+\Lambda M'\right)\ddot{q}-\left(V'+\Lambda V'\right)\dot{q}-V'\ddot{q}\right.\\ &\left.+M\left(\ddot{q}-\ddot{q}_d+\Lambda_1\ddot{e}+\Lambda_2\dot{e}\right)+V'\left(\ddot{e}+\Lambda_1\dot{e}+\Lambda_2 e\right)\right]\\ &= s^T\left[\Lambda u+M\left(\Lambda_1\ddot{e}+\Lambda_2\dot{e}-\ddot{q}_d\right)+V'\left(\Lambda_1\dot{e}+\Lambda_2 e-\ddot{q}_d\right)\right.\\ &\left.-\left(\dot{M}'+\Lambda M'\right)\ddot{q}-\left(V'+\Lambda V'\right)\dot{q}\right] = s^T(\Lambda u+H)\end{aligned} \tag{19}$$

where $H = M(\Lambda_1\ddot{e}+\Lambda_2\dot{e}-\ddot{q}_d)+V'(\Lambda_1\dot{e}+\Lambda_2 e-\ddot{q}_d) -\left(\dot{M}'+\Lambda M'\right)\ddot{q}-\left(V'+\Lambda V'\right)\dot{q}]$.

Based on the linear characteristics described as Eq. (13), $H = \Gamma(t,q,\dot{q},\ddot{q},q_d,\dot{q}_d,\ddot{q}_d,\ddot{q}_d)\phi$, where ϕ is the unknown vector. If there exists a known vector ϕ_0, satisfy the condition as $|\tilde{\phi}_i| = |\phi_i-\phi_{0i}|\le\xi_i$, where $\xi_i>0$ and $i=1,2,\ldots,n$. Then, $\dot{L} = s^T(\Lambda u+\Gamma\phi)$.

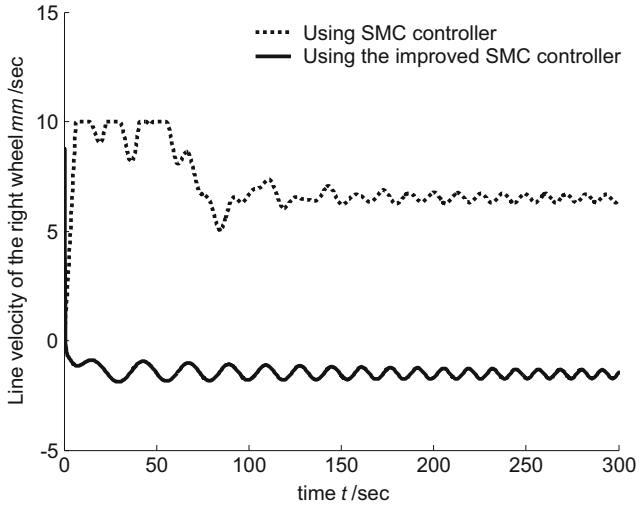

(a) Velocity of the right wheel

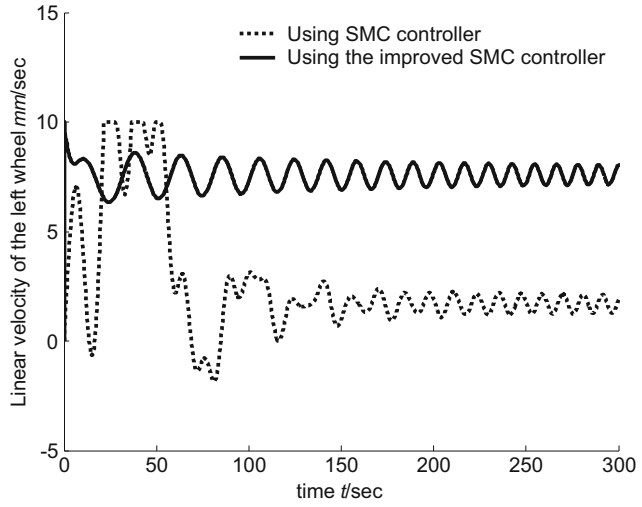

(b) Velocity of the left wheel

Fig. 13 Velocity of the right (**a**) and left (**b**) drive wheels

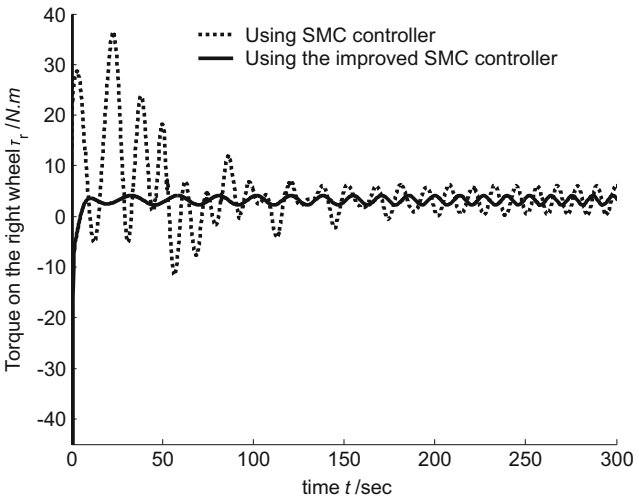

(a) Torque on the right wheel

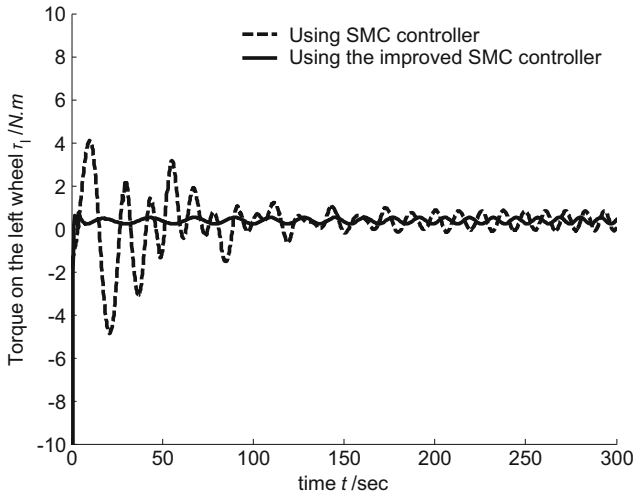

(b) Torque on the left wheel

Fig. 14 Torque on the right (**a**) and left (**b**) drive wheels

Design the sliding mode control law as follows:

$$u = -\Lambda^{-1}\left[\Gamma\phi_0 + \left(\overline{\Gamma}\xi\right)\mathrm{sgn}(s) - \psi\mathrm{sgn}(s)\right] \tag{20}$$

where $\Gamma\phi_0 = H_0$, in which H_0 is the precise model of H; $\overline{\Gamma}_{ij} = \left|\Gamma_{ij}\right|$; $\psi = \mathrm{diag}(\psi_1, \psi_2, \ldots, \psi_n)$; $\psi_i > 0, \quad i = 1, 2, \ldots, n$; $\mathrm{sgn}(s) = [\mathrm{sgn}(s_1), \mathrm{sgn}(s_2), \ldots, \mathrm{sgn}(s_n)]$. Then, Eq. (18) is written as

$$\begin{aligned}\dot{L} &= s^T\left[\Gamma(\phi - \phi_0) - \left(\overline{\Gamma}\xi\right)\mathrm{sgn}(s) - \psi\mathrm{sgn}(s)\right] \\ &= s^T\left[\Gamma\tilde{\phi} - \left(\overline{\Gamma}\xi\right)\mathrm{sgn}(s) - \psi\mathrm{sgn}(s)\right] \\ &= \sum_{i=1}^{n}\left\{s_i\left(\Gamma\tilde{\phi}\right)_i - |s_i|\left(\Gamma\tilde{\phi}\right)_i\right\} - s^T\psi\mathrm{sgn}(s) \le -s^T\psi\mathrm{sgn}(s) \\ &= -\sum_{i=1}^{n}(\psi_i|s_i|) \le 0\end{aligned} \tag{21}$$

Assumed $\eta = \overline{\Gamma}\xi\psi$, the sliding mode control law (Eq. (20)) can be rewritten as

$$u = -\Lambda^{-1}[\Gamma\phi_0 + \eta\mathrm{sgn}(s)] \tag{22}$$

In order to completely eliminate the chattering, the SGN function is replaced by using the unit vector continuous function as [15]. Then, the control law become

$$u = -\Lambda^{-1}\left[\Gamma\varphi_0 + \eta\frac{ks}{\|s\| + \delta}\right] \tag{23}$$

where $\delta \in R^{2\times 1}$ is the smooth parameter in regulating the switching function and $\delta > 0$. k is time varying, whose change can represent the change of the uncertain term [15], and $k \ge \frac{\left\|\Delta A A^{-1}(\hat{v} - H)\right\| + \|\Delta H\| + \mu}{1 - \left\|\Delta A A^{-1}\mathrm{sgn}s\right\|}$ ($\mu > 0$), where A, ΔA, H, and ΔH are coefficient matrixes related to the welding robot structure; $\hat{v}$ is the equivalent control.

7 Verification program

In order to verify the correctness and effectiveness of this algorithm, the mobile welding robot is required to track reference trajectories. In the process, the dynamic model described in Eq. (5) is used as the mobile welding robot mode. The expectation velocity, angular speed, and sampling time are 10 mm/s, 0.02 rad/s, and 0.2 s, respectively.

The tracking velocities, linear velocity of the welding torch, control output, and velocity of the two wheels using a traditional low-pass filter and an improved low-pass filter are shown in Figs. 9, 10, 11, 12, 13, and 14, respectively. Figure 9 shows that the errors using the improved low-pass filter are less than those using the traditional sliding mode control. The linear velocity of the welding torch using the improved low-pass filter is relatively more stable than that using the traditional sliding mode control (shown in Fig. 11).

From Figs. 9, 10, 11, 12, 13, and 14, we can see that the proposed method yields a superior performance such as small seam tracking error and high resistance behavior to noise uncertainties. And the tracking performance of the mobile welding robot under the control of the improved method is better than that of the traditional method.

8 Conclusion

We conducted simulation and experiment to verify the validity of the derived mathematical model and the capability of the robot in seam tracking a predefined path.

(1) One control method is proposed for automatic finding of the position of the welding line. The sensor system detects the position and groove shape of the welding line, and the control system is designed to calculate the entrance angle and the width of the groove. The turning locomotion is composed of three-stage Fresnel functions aimed at finding the position of the weld line.
(2) In order to weaken the chattering phenomena, the first-order low-pass filter (LPF) has been used in the controller design of mobile welding robot. The LPF was used to eliminate the high-frequency chattering control signal. In order to further weaken the influence of the chattering and increase the precise of the trace tracking of the mobile welding robot, the traditional switching function is instead replaced by smooth continuous function
(3) The proposed method has the ability to solve the seam tracking problem based on the dynamic modeling of the mobile welding robot. The experiment results show that the proposed method yields a superior performance such as small seam tracking error and high-precision linear velocity.

Acknowledgments This project was supported by the National Natural Science Foundation of China (Grant No. 51405286) and Shanghai Key Laboratory Power Station Automation Technology Laboratory (Grant No. 13DZ2273800).

References

1. Xu PQ TXH, LU FG, Yao S (2007) An active vision sensing method for welded seams location using "circle-depth relation" algorithm. Int J Adv Manuf Tech 32(9):918–926. doi:10.1007/s00170-006-0410-0
2. Chang DY, Son DH, Lee JW, Lee DH, Kim TW, Lee KY, Kim JW (2012) A new seam-tracking algorithm through characteristic-point detection for a portable welding robot. Robot Comput Integr Manuf 28:1–13. doi:10.1016/j.rcim.2011.06.001

3. Zheng R, Zhang P, Aiqing D, Peng X (2014) Measurement of laser welding pool geometry using a closed convex active contour model. Meas Sci Technol 25:035010. doi:10.1088/0957-0233/25/3/035603 (17pp)
4. Gregor G¨o, Heinz Sch¨opp FH, Gerd H (2010) Improvement of the control of a gas metal arc welding process. Meas Sci Technol 21(2):025201. doi:10.1088/0957-0233/21/2/025201
5. Huang Y, Xiao YL, Wang PJ, Li MZH (2013) A seam-tracking laser welding platform with 3D and 2D visual information fusion vision sensor system. Int J Adv Manuf Technol 67(1):415–426. doi:10.1007/s00170-012-4494-4
6. Heber M, Lenz M, Rüther M, Bischof H, Fronthaler H, Croonen G (2013) Weld seam tracking and panorama image generation for on-line quality assurance. Int J Adv Manuf Technol 65(9):1371–1382. doi:10.1007/s00170-012-4263-4
7. Nele L, Sarno E, Keshari A (2013) An image acquisition system for real-time seam tracking. Int J Adv Manuf Technol 69(9):2099–2110. doi:10.1007/s00170-013-5167-7
8. Shao JY, Zhang CQ, Liu Z, CHEN K (2012) Trajectory optimization method of special operation redundant root for vibration suppression. J Mech Eng 48(1):1–7. doi:10.3901/JME.2012.01.013
9. Yang SM, Cho MH, Lee HY, Cho TD (2007) Weld line detection and process control for welding automation. Meas Sci Technol 18(3):819–826. doi:10.1088/0957-0233/18/3/034
10. Aghili F (2012) A prediction and motion-planning scheme for visually guided robotic capturing of free-floating tumbling objects with uncertain dynamics. IEEE Trans Robot 28(3):634–649. doi:10.1109/TRO.2011.2179581
11. Pan BZH, Song YM, Wang PF, Dong G, Sun T (2014) Laser tracker based rapid home position calibration of a hybrid robot. J Mech Eng 50(1):31–37. doi:10.3901/JME.2014.01.031
12. Gao SH, Chang YL, ZHang RJ, Ren YL (2008) Space welding seam tracking based on free floating space robot. Transactions of the China Welding Institution 29(11):65–68. doi:10.3321/j.issn:0253-360X.2008.11.017
13. Hong B, Zhang QL, Li XW, Li Y (2012) A analysis method of seam tracking accuracy based on wheeled robot. Transactions of the China Welding Institution 33(1):13–16
14. Wand ZY, Li YD, Zhu L (2010) Dual adaptive neural sliding mode control of nonholonomic mobile robot. J Mech Eng 46(23):16–22. doi:10.3901/JME.2010.23.016
15. Wu B, Xu WF, CHen HL (2009) Application of neural networks sliding mode control in tracking control of robot manipulators. Electric Machines and Control 13(sup1):99–104. doi:10.15938/j.emc.2009.s1.029
16. Wu M, Li LL, Sun JY (2012) PDA-IMM based moving object tracking with mobile robots in unknown environments. Robot 34(6):668–679. doi:10.3724/SP.J.1218.2012.00668
17. Zhang T, Chen SB (2014) Optimal posture searching algorithm on mobile welding robot. J Shanghai Jiaotong Univ (Sci) 19(1):84–87. doi:10.1007/s12204-014-1477-7
18. Wei C, Zhao Y, Wang HL (2011) Space robot soft-hard grasping based on sliding mode control. J Mech Eng 47(1):43–47. doi:10.3901/JME.2011.01.043, 54
19. Jaime F, Aviles-Viñas RRC, Ismael LJ (2016) On-line learning of welding bead geometry in industrial robots. Int J Adv Manuf Technol 83(1):217–231. doi:10.1007/s00170-015-7422-6
20. Shi L, Tian XC, Zhang CH (2015) Automatic programming for industrial robot to weld intersecting pipes. Int J Adv Manuf Technol 81(9):2099–2107. doi:10.1007/s00170-015-7331-8
21. Gao XD, Mo L, Xiao ZL, Chen XH, Katayama S (2016) Seam tracking based on Kalman filtering of micro-gap weld using magneto-optical image. Int J Adv Manuf Technol 83(1):21–32. doi:10.1007/s00170-015-7560-x
22. Chen HY, Liu K, Xing GS, Dong Y, Sun HX, Lin W (2013) A robust visual servo control system for narrow seam double head welding robot. Int J Adv Manuf Technol 71(9):1849–1860. doi:10.1007/s00170-013-5593-6
23. Qiao JF (2014) Design of liquid concentration measurement system based on single chip microcomputer. Taiyuan Industrial College, Master's degree thesis
24. Lu XQ, Zhang K, Liu G, Wu YX (2007) The control of a mobile robot to find the weld line automatically. Weld Cut 6(6):334–338
25. Lü XQ, Zhang K, Wu YX (2014) Control of the wheeled mobile welding robot based on output feedback linearization. J mech Eng 50(6):48–54. doi:10.3901/JME.2014.06.048
26. Chen Y, Zhang JF, Yang CJ, Niu B (2007) Design and hybrid control of the pneumatic force-feedback systems for arm-exoskeleton by using on/off valve. Mech Mater 17(7):325–335. doi:10.1016/j.mechatronics.2007.04.001
27. Chen Y, Zhang JF, Yang CJ, Niu B (2007) The workspace mapping with deficient DOF space for the puma 560 robot and its exoskeleton arm by using orthogonal experiment design method. Robot Comput Integr Manuf 23(4):478–487. doi:10.1016/j.rcim.2006.05.007
28. Zhang X, Liu FJ, Yan MD (2012) Dynamic model-based adaptive sliding-mode trajectory tracking control over wheeled mobile robot. Mechanical Science and Technology for Aerospace Engineering 31(1):107–112. doi:10.13433/j.cnki.1003-8728.2012.01.018
29. Zhu JW, Zhu DC, Cai JB (2009) Design of sliding mode controller with low-pass filter for robot manipulators. Second International Workshop on Knowledge Discovery and Data Mining, Date of Conference: 23-25 Jan. 2009, Conference Location: Moscow, pp. 296-298. doi: 10.1109/WKDD.2009.118
30. Jin X, Huang J, Zhang K, Wu YX (2011) Kinematics modeling and real-time seam tracking for welding mobile robot. Second International Conference on Digital Manufacturing & Automation, Issue Date: 5-7 Aug, pp. 681-685. doi: 10.1109/ICDMA.2011.170
31. ZHang K, Wu YX, Lu XQ, Jin X (2008) Dynamic modeling for differentially steered welding mobile robot. J Mech Eng 44(11):116–120. doi:10.3901/JME.2008.11.116